Synergistic plasmonic and photonic crystal light-trapping: Architectures for optical up-conversion in thin-film solar cells

Khai Q. Le[1,3,*] and Sajeev John[1,2]

[1]*Department of Physics, University of Toronto, Toronto, ON M5S 1A7, Canada*
[2]*Department of Physics, King Abdulaziz University, Jeddah, Saudi Arabia*
[3]*Faculty of Science and Technology, Hoa Sen University, Ho Chi Minh, Vietnam*
[*]*khaidotle@gmail.com*

Abstract: We demonstrate, numerically, that with a 60 nanometer layer of optical up-conversion material, embedded with plasmonic core-shell nano-rings and placed below a sub-micron silicon conical-pore photonic crystal it is possible to absorb sunlight well above the Lambertian limit in the 300-1100 nm range. With as little as 500 nm, equivalent bulk thickness of silicon, the maximum achievable photo-current density (MAPD) is about 36 mA/cm^2, using above-bandgap sunlight. This MAPD increases to about 38 mA/cm^2 for one micron of silicon. Our architecture also provides solar intensity enhancement by a factor of at least 1400 at the sub-bandgap wavelength of 1500 nm, due to plasmonic and photonic crystal resonances, enabling a further boost of photo-current density from up-conversion of sub-bandgap sunlight. With an external solar concentrator, providing 100 suns, light intensities sufficient for significant nonlinear up-conversion can be realized. Two-photon absorption of sub-bandgap sunlight is further enhanced by the large electromagnetic density of states in the photonic crystal at the re-emission wavelength near 750 nm. It is suggested that this synergy of plasmonic and photonic crystal resonances can lead to unprecedented power conversion efficiency in ultra-thin-film silicon solar cells.

OCIS codes: (350.6050) Solar energy; (350.4238) Nanophotonics and photonic crystals; (240.6680) Surface plasmons; (040.5350) Photovoltaic; (250.5403) Plasmonics.

References and Links

1. T. Saga, "Advances in crystalline silicon solar cell technology for industrial mass production," NPG Asia Mater. **2**(3), 96–102 (2010).
2. K. R. Catchpole and A. Polman, "Plasmonic solar cells," Opt. Express **16**(26), 21793–21800 (2008).
3. S. Hänni, G. Bugnon, G. Parascandolo, M. Boccard, J. Escarré, M. Despeisse, F. Meillaud, and C. Ballif, "High-efficiency microcrystalline silicon single-junction solar cells," Prog. Photovolt. Res. Appl. **21**(5) 821–826(2013).
4. S. E. Han and G. Chen, "Toward the Lambertian limit of light trapping in thin nanostructured silicon solar cells," Nano Lett. **10**(11), 4692–4696 (2010).
5. A. Abass, K. Q. Le, A. Alù, M. Burgelman, and B. Maes, "Dual-interface gratings for broadband absorption enhancement in thin-film solar cells," Phys. Rev. B **85**(11), 115449 (2012).
6. U. W. Paetzold, E. Moulin, D. Michaelis, W. Böttler, C. Wächter, V. Hagemann, M. Meier, R. Carius, and U. Rau, "Plasmonic reflection grating back contacts for microcrystalline silicon solar cells," Appl. Phys. Lett. **99**(18), 181105 (2011).
7. W. Wang, S. Wu, K. Reinhardt, Y. Lu, and S. Chen, "Broadband light absorption enhancement in thin-film silicon solar cells," Nano Lett. **10**(6), 2012–2018 (2010).
8. P. Spinelli, V. E. Ferry, J. van de Groep, M. van Lare, M. A. Verschuuren, R. E. I. Schropp, H. A. Atwater, and A. Polman, "Plasmonic light trapping in thin-film Si solar cells," J. Opt. **14**(2), 024002 (2012).
9. K. Q. Le, A. Abass, B. Maes, P. Bienstman, and A. Alù, "Comparing plasmonic and dielectric gratings for absorption enhancement in thin-film organic solar cells," Opt. Express **20**(S1), A39–A50 (2012).

10. S. John, "Electromagnetic absorption in a disordered medium near a photon mobility edge," Phys. Rev. Lett. **53**(22), 2169–2172 (1984).
11. E. Yablonovitch, "Inhibited spontaneous emission in solid-state physics and electronics," Phys. Rev. Lett. **58**(20), 2059–2062 (1987).
12. S. John, "Strong localization of photons in certain disordered dielectric superlattices," Phys. Rev. Lett. **58**(23), 2486–2489 (1987).
13. S. John, "Why trap light?" Nat. Mater. **11**(12), 997–999 (2012).
14. M. Green, *Third Generation Photovoltaics* (Springer, 2006).
15. S. Foster and S. John, "Light-trapping in dye-sensitized solar cells," Energy Environ. Sci. **6**, 2972–2983 (2013).
16. X. Meng, V. Depauw, G. Gomard, O. El Daif, C. Trompoukis, E. Drouard, C. Jamois, A. Fave, F. Dross, I. Gordon, and C. Seassal, "Design, fabrication and optical characterization of photonic crystal assisted thin film monocrystalline-silicon solar cells," Opt. Express **20**(S4 Suppl 4), A465–A475 (2012).
17. L. Zeng, Y. Yi, C. Hong, J. Liu, N. Feng, X. Duan, L. C. Kimerling, and B. A. Alamariu, "Efficiency enhancement in Si solar cells by textured photonic crystal back reflector," Appl. Phys. Lett. **89**(11), 111111 (2006).
18. G. Demésy and S. John, "Solar energy trapping with modulated silicon nanowire photonic crystals," J. Appl. Phys. **112**(7), 074326 (2012).
19. A. Deinega and S. John, "Solar power conversion efficiency in modulated silicon nanowire photonic crystals," J. Appl. Phys. **112**(7), 074327 (2012).
20. E. Garnett and P. Yang, "Light trapping in silicon nanowire solar cells," Nano Lett. **10**(3), 1082–1087 (2010).
21. X. X. Lin, X. Hua, Z. G. Huang, and W. Z. Shen, "Realization of high performance silicon nanowire based solar cells with large size," Nanotechnology **24**(23), 235402 (2013).
22. C. Lin and M. L. Povinelli, "Optimal design of aperiodic, vertical silicon nanowire structures for photovoltaics," Opt. Express **19**(S5), A1148–A1154 (2011).
23. L. Hu and G. Chen, "Analysis of optical absorption in silicon nanowire arrays for photovoltaic applications," Nano Lett. **7**(11), 3249–3252 (2007).
24. A. Chutinan and S. John, "Light trapping and absorption optimization in certain thin-film photonic crystal architectures," Phys. Rev. A **78**(2), 023825 (2008).
25. E. Yablonovitch, "Statistical ray optics," J. Opt. Soc. Am. **72**(7), 899–907 (1982).
26. S. Eyderman, S. John, and A. Deinega, "Solar light trapping in slanted conical-pore photonic crystals: Beyond statistical ray trapping," J. Appl. Phys. **113**(15), 154315 (2013).
27. A. Deinega, S. Eyderman, and S. John, "Coupled optical and electrical modeling of solar cell based on conical pore silicon photonic crystals," J. Appl. Phys. **113**(22), 224501 (2013).
28. Y. C. Chen and T. M. Chen, "Improvement of conversion efficiency of silicon solar cells using up-conversion molybdate La$_2$Mo$_2$O$_9$:Yb, R (R=Er, Ho) phosphors," J. Rare Earths **29**(8), 723–726 (2011).
29. Z. R. Abrams, A. Niv, and X. Zhang, "Solar energy enhancement using down-converting nanoparticles: A rigorous approach," J. Appl. Phys. **109**(11), 114905 (2011).
30. S. Fischer, F. Hallermann, T. Eichelkraut, G. von Plessen, K. W. Krämer, D. Biner, H. Steinkemper, M. Hermle, and J. C. Goldschmidt, "Plasmon enhanced upconversion luminescence near gold nanoparticles-simulation and analysis of the interactions," Opt. Express **20**(1), 271–282 (2012).
31. T. Trupke, M. A. Green, and P. Wurfel, "Improving solar cell efficiencies by up-conversion of sub-band-gap light," J. Appl. Phys. **92**(7), 4117–4122 (2002).
32. J. C. C. Fan, "The future of high efficiency solar cells," Sol. Cells **12**(1-2), 51–62 (1984).
33. M. F. Lamorte and D. Abbot, "Analysis of AlGaAs–GaInAs cascade solar cell under AM0–AM5 spectra," Solid-State Electron. **22**(5), 467–473 (1979).
34. F. A. Rubinelli, J. K. Rath, and R. E. I. Schropp, "Microcrystalline n-i-p tunnel junction in a-Si:H/a-Si:H tandem cells," J. Appl. Phys. **89**(7), 4010 (2001).
35. R. P. Gale, J. C. C. Fan, G. W. Turner, R. L. Chapman, and J. V. Pantato, "Efficient AlGaAs shallow-homojunction solar cells," Appl. Phys. Lett. **44**(6), 632–634 (1984).
36. M. J. Keevers and M. A. Green, "Efficiency improvements of silicon solar cells by the impurity photovoltaic effect," J. Appl. Phys. **75**(8), 4022–4031 (1994).
37. G. Gutler and H. Queisser, "Impurity photovoltaic effect in silicon," Energy Convers. **10**(2), 51–55 (1970).
38. W. Shockley and H. J. Queisser, "Detailed balance limit of efficiency of p-n junction solar cells," J. Appl. Phys. **32**(3), 510–519 (1961).
39. T. Trupke, A. Shalav, B. S. Richards, P. Wurfel, and M. A. Green, "Efficiency enhancement of solar cells by luminescent up-conversion of sunlight," Sol. Energy Mater. Sol. Cells **90**(18-19), 3327–3338 (2006).
40. P. Gipart, F. Auzel, J.-C. Guillaume, and K. Zahraman, "Below band-gap IR response of substrate-free GaAs solar cells using two-photon up-conversion," Jpn. J. Appl. Phys. **35**(8), 4401–4402 (1996).
41. S. Fischer, J. C. Goldschmidt, P. Loper, G. H. Bauer, K. W. Kramer, D. Biner, M. Hermle, and S. W. Glunz, "Enhancement of silicon solar cell efficiency by upconversion: optical and electrical characterization," J. Appl. Phys. **108**(4), 044912 (2010).
42. W. Zou, C. Visser, J. A. Maduro, M. S. Pshenichnikov, and J. C. Hummelen, "Broadband dye-sensitized upconverion of near-infrared light," Nat. Photonics **6**(8), 560–564 (2012).
43. S. Schietinger, T. Aichele, H.-Q. Wang, T. Nann, and O. Benson, "Plasmon-enhanced upconversion in single NaYF$_4$:Yb^{3+}/Er^{3+} codoped nanocrystals," Nano Lett. **10**(1), 134–138 (2010).

44. A. C. Atre, A. G. Etxarri, H. Alaeian, and J. A. Dionne, "Toward high-efficiency solar upconversion with plasmonic nanostructures," J. Opt. **14**(2), 024008 (2012).
45. J.-Ch. Boyer and F. C. J. M. van Veggel, "Absolute quantum yield measurements of colloidal NaYF$_4$: Er^{3+}, Yb^{3+} upconverting nanoparticles," Nanoscale **2**(8), 1417–1419 (2010).
46. A. Shalav, B. S. Richards, and M. A. Green, "Luminescent layers for enhanced silicon solar cell performance: up-conversion," Sol. Energy Mater. Sol. Cells **91**(9), 829–842 (2007).
47. E. D. Palik, *Handbook of Optical Constants of Solids* (Academic Press, 1985).
48. P. B. Johnson and R. W. Christy, "Optical constants of the noble metals," Phys. Rev. B **6**(12), 4370–4379 (1972).
49. S. Fischer, H. Steinkemper, P. Loper, M. Hermle, and J. C. Goldschmidt, "Modeling upconversion of erbium doped nanocrystals based on experimentally determined Einstein coefficients," J. Appl. Phys. **111**(1), 013109 (2012).
50. A. Abass, H. Shen, P. Bienstman, and B. Maes, "Angle insensitive enhancement of organic solar cells using metallic gratings," J. Appl. Phys. **109**(2), 023111 (2011).
51. H. Shen, P. Bienstman, and B. Maes, "Plasmonic absorption enhancement in organic solar cells with thin active layers," J. Appl. Phys. **106**(7), 073109 (2009).
52. R. Ren, Y. Guo, and R. Zhu, "Design of a plasmonic back reflector for silicon nanowire decorated solar cells," Opt. Lett. **37**(20), 4245–4247 (2012).
53. A. Mellor, H. Hauser, C. Wellens, J. Benick, J. Eisenlohr, M. Peters, A. Guttowski, I. Tobías, A. Martí, A. Luque, and B. Bläsi, "Nanoimprinted diffraction gratings for crystalline silicon solar cells: implementation, characterization and simulation," Opt. Express **21**(S2 Suppl 2), A295–A304 (2013).
54. K. Zhou, Z. Guo, X. Li, J. Y. Jung, S. W. Jee, K. T. Park, H. D. Um, N. Wang, and J. H. Lee, "The tradeoff between plasmonic enhancement and optical loss in silicon nanowire solar cells integrated in a metal back reflector," Opt. Express **20**(S5 Suppl 5), A777–A787 (2012).
55. F. Auzel, "Upconversion and anti-Stokes processes with f and d ions in solids," Chem. Rev. **104**(1), 139–174 (2004).
56. F. Wang and X. Liu, "Recent advances in the chemistry of lanthanide-doped upconversion nanocrystals," Chem. Soc. Rev. **38**(4), 976–989 (2009).
57. D. R. Gamelin and H. U. Güdel, "Design of luminescent inorganic materials: new photophysical processes studied by optical spectroscopy," Acc. Chem. Res. **33**(4), 235–242 (2000).
58. V. K. Rai, C. B. de Araújo, Y. Ledemi, B. Bureau, M. Poulain, X. H. Zhang, and Y. Messaddeq, "Surface-plasmon-enhanced frequency upconversion in Pr^{3+} doped tellurium-oxide glasses containing silver nanoparticles," J. Appl. Phys. **103**(9), 093526 (2008).
59. J. C. Goldschmidt, S. Fisher, H. Steinkemper, F. Hallermann, G. von Plessen, K. W. Kramer, D. Biner, and M. Hermle, "Increasing upconversion by plasmon resonance in metal nanoparticles-A combined simulation analysis," IEEE J. Photovolt. **2**(2), 134–140 (2012).
60. K.-Y. Jung, F. L. Teixeira, and R. M. Reano, "Au/SiO2 nanoring plasmon waveguides at optical communication band," J. Lightwave Technol. **25**(9), 2757–2765 (2007).

1. Introduction

Crystalline silicon (c-Si) is the most widely used material for single junction solar cells [1]. However, due to its indirect electronic bandgap and poor absorption efficiency in the red to near-infrared spectrum, most commercial c-Si solar cells utilize wafers with a thickness of a few hundred microns (100-300 μm). This accounts for about 40% of the final module cost [2]. Efforts to reduce the cost of energy production utilize thin-film photovoltaic (PV) cells with an equivalent active layer thickness of about 1-3 μm [3]. In such thin films it is essential to optimize light-trapping [4] and antireflection [5] in order to achieve power conversion efficiencies comparable to thick wafers. Engineering the back reflector of the solar cell [6,7] and integrating plasmonic nanostructures [8] in the active layer to excite localized surface plasmon resonances (LSPRs) can also improve sunlight absorption through near-field enhancement effects [9]. Solar light-trapping for efficient absorption in thin films relies on the engineering of an enhanced electromagnetic density of states and is distinct from the concept of light localization [10] in a suppressed electromagnetic density of states such as a photonic band gap [11−13]. Instead, slow-light modes in the higher bands of certain photonic crystals (PC's) provide a unique opportunity for light management in third generation solar cells [14]. Thin-film PC-based solar cells have been considered in 1D, 2D and 3D periodic structures [15−19].

Nanowire photonic crystal arrays of various forms and shapes have attracted much attention since they exhibit several light-trapping effects. A radial P-N junction geometry in

silicon nanowire solar cells results in rapid separation of electrons and holes throughout the active light-trapping region, reducing recombination losses and contributing to high power conversion efficiency [20–24]. However, silicon nanowires optimized for both light trapping and antireflection surpass the Lambertian light-trapping [25,26] only over a partial spectral range [4] but not over the broader spectrum from 300 to 1100 nm.

Recently, a silicon PC, consisting of slanted conical pores that can trap and absorb sunlight beyond the Lambertian limit over the entire solar spectrum was introduced [26]. This architecture combines both an antireflective graded index and PC light-trapping to achieve exceptional solar absorption in silicon films as thin as 380 nm (equivalent bulk thickness). With 1 μm of c-Si placed on a silver (Ag) back reflector, the slanted conical pore PC provides a maximum achievable photocurrent density (MAPD) of 35.5 mA/cm^2, exceeding the Lambertian limit of 32.6 mA/cm^2 over the integrated wavelength range of 300-1100 nm. Through coupled electrical and optical simulations, this single-junction solar cell structure was shown to provide solar power conversion efficiency (at one sun intensity) between 17.5% and 22.5%, depending on the surface recombination velocity at the back contact [27].

The slanted conical pore silicon PC is capable of higher power conversion efficiency if nonlinear solar spectrum reshaping effects (up-conversion [28] or down-conversion [29]) enabled by strong light focusing are exploited. A significant power loss in single bandgap solar cells is due to their non-utilization of sub-bandgap sunlight. Roughly 20% of the incident solar power is not harnessed in silicon photovoltaic cells because low-energy photons below the bandgap of silicon do not carry enough energy to generate free charge carriers [30,31]. Efforts to make use of this otherwise lost part of the solar spectrum have attracted considerable interest. One approach is to fabricate multi-junction, tandem solar cells [32,33], in which cells consisting of different semiconductors are stacked and separated by tunnel junctions [34]. The top cell is used to absorb the UV and visible light and lower cells, with successively lower bandgaps, absorb longer wavelength sunlight [35]. For example, overall efficiency in a two-cell device is maximized if the energy gaps (Eg) of the top cell and the bottom cell are approximately 1.75-1.80 eV and 1.0-1.1 eV, respectively. It was shown [35] in this case that the maximum practical power conversion efficiency under AM1 conditions is increased to 30% compared to about 23% for single-junction cells. However, multi-junction cells involve greater complexity and cost compared to their single-junction counterparts. Impurity photovoltaic (IPV) silicon solar cells have also been proposed [36] in which the insertion of impurities increases the infrared (IR) photon absorption in a multistep process. Such IPV cells introduce defect states within the semiconductor bandgap that often produce additional pathway for recombination, limiting its practical energy conversion efficiency [37].

In an up-conversion (UC) solar cell, only a single P-N junction is required and two low-energy sub-bandgap photons are absorbed and re-emitted into the active region as a single photon above the semiconductor bandgap in a nonlinear process. It has been suggested [30] that UC can enhance the maximum allowable thermodynamic power conversion efficiency [38] of a single-junction silicon solar cell from 30% to over 40% [39]. Two-photon UC in solar cell structures was first demonstrated by Gibart et al. [40]. In these solar cells, the UC layer is placed below the active photo-current generation layer. However, since UC is based on a nonlinear optical effect, light intensities on the order of 10^5 suns are required to achieve substantial yield.

In this paper, we introduce a combined plasmonic and thin-film photonic crystal architecture that provides linear light absorption well beyond the Lambertian limit and at the same time provides light focusing in the nonlinear UC layer in excess of 10^3 suns, without recourse to a solar concentrator. A thin (60 nm) layer containing hexagonal sodium yttrium fluoride (β-NaYF$_4$) doped with trivalent erbium (Er^{3+}) sandwiched between the silicon light trapping PC layer and the Ag back-reflector can up-convert near-infrared (NIR) photons at wavelengths around 1523 nm [30,41]. It is also useful to sensitize such Er-nanocrystals with dye-molecule antennae that absorb sub-bandgap sunlight in the range of 1100-1500 nm and

down-convert sunlight throughout this range to the wavelength required for two-photon up-conversion by Erbium [42]. Interestingly, we find that a thin UC layer, suitably placed, also enhances linear absorption of above-bandgap sunlight by reducing parasitic absorption losses in the Ag back reflector.

The major drawback of UC is its low quantum yield with the use of conventional solar concentrators. Very high local light intensity is required to drive the nonlinear optical UC process. Efforts to improve the UC efficiency have utilized metallic nanoparticles placed near the up-converting material to enhance up-converted fluorescence [43] and metallic nano-shells with up-converter-doped dielectric cores to provide strong electromagnetic field concentration in the cores [44]. However, these light-focusing resonances are mostly located in the 600-760 nm spectral range, with limited relevance to silicon solar cell applications. The highest UC quantum yield of the most widely used up-converting materials under laser irradiation occurs at wavelengths around 975 nm and 1523 nm [41,45,46]. To place plasmonic resonances at such NIR wavelengths and thereby amplify the UC quantum yield, we introduce core-shell rings on the Ag back reflector that protrude into the UC layer. Here, the core consists of up-converting materials (β-NaEr$_{0.2}$Y$_{0.8}$F$_4$) and the shell is made of Ag. The frequencies of the resulting plasmonic resonances can be varied throughout the NIR range by adjusting the radii of the metallic rings.

Interestingly, we find that our core-shell ring plasmonic resonators and UC layer reduce absorption losses in the Ag back reflector, enhance overall light-trapping and provide MAPD enhancement from above-gap, single-photon absorption in the overlying silicon photonic crystal. Moreover, the NIR light intensity in specific regions of the UC layer is enhanced by a factor of 1.4×10^3 at desired wavelengths. This provides opportunities to enhance low-power up-conversion of sub-gap sunlight for greater overall power conversion efficiency.

In Section 2, we will describe a solar cell structure and simulation details. In section 3, MAPD enhancement by a thin up-conversion layer is presented. Section 4 shows enhanced light trapping and plasmonic field enhancement by core-shell rings followed by conclusions in Section 5.

2. Solar cell structure and simulation details

A single unit cell of the slanted conical-pore PC structure is depicted in Fig. 1. The active layer is made of c-Si and periodically patterned with slanted conical pores. The metallic back-contact (back reflector) consists of Ag. This provides low metal absorption loss and, when suitably structured, offers surface plasmon resonance modes needed for strong field enhancement in the up-conversion layer. Our simulations are carried out using previously optimized [26] slanted conical-pore photonic crystal parameters. For an equivalent bulk thickness of 1.0 microns of silicon, the lattice constant a = 850 nm, cone radius R = 425 nm and cone height h = 1.6 μm. For smaller volumes of silicon, we simply reduce the cone height while keeping the other parameters fixed. Indeed the most cost effective choice for the equivalent bulk thickness of silicon is about 380 nm (h = 600 nm) for which the MAPD of 33.4 mA/cm^2 is reduced by only 12% relative to the solar cell with 1.0 microns of silicon. Refractive indices of c-Si and Ag are taken from [47] and [48], respectively, while the dielectric constant of β-NaEr$_{0.2}$Y$_{0.8}$F$_4$ is 1.5 and its absorption coefficient is extracted from [49].

For our periodic device structure, only one unit cell with a lattice constant a is required for the computational domain with proper periodic boundary conditions. Numerical simulations are carried out by the 3D finite element method [5,9,50,51]. For calculated angular dependence of the light absorption, Floquet-Bloch periodic boundary conditions are implemented at the left and right boundaries, while perfectly matched layer absorbing boundary conditions are used at the top and bottom boundaries of the computational domain. The optical absorption A(λ) is calculated by integrating the divergence of the Poynting vector (power flow) which is then normalized with input power over one period. To quantify the

absorption of the sunlight, the absorption spectrum is then integrated over the wavelength range of 300-1100 nm weighted by the AM1.5G solar spectrum. It results in the so-called integrated absorption efficiency [50]:

$$AE_{Int} = \frac{\int\limits_{300nm}^{1100nm} A(\lambda) \times AM1.5G(\lambda) d\lambda}{\int\limits_{300nm}^{1100nm} AM1.5G(\lambda) d\lambda}.$$

(1)

The maximum achievable photocurrent density (MAPD), in which all generated carriers are assumed to be collected, is calculated by integrating the optical absorption A(λ) with the incident AM1.5G solar spectrum over the desired wavelength range of 300-1100 nm:

$$MAPD = \int\limits_{300nm}^{1100nm} \frac{e\lambda}{hc} A(\lambda) \times AM1.5G(\lambda) d\lambda.$$

(2)

Here, h is Planck's constant, e is the electronic charge and c is the speed of light in vacuum. The MAPD is an alternative measure of the total amount of the sunlight absorbed in a given structure. Assuming that each absorbed photon translates into a single electron-hole pair that is collected without electron-hole recombination losses, the MAPD is equivalent to the maximum achievable short circuit current density. For example: with 100% absorption of the AM1.5G sunlight integrated over the wavelength range of 300-1100 nm, the MAPD is 43.5 mA/cm^2.
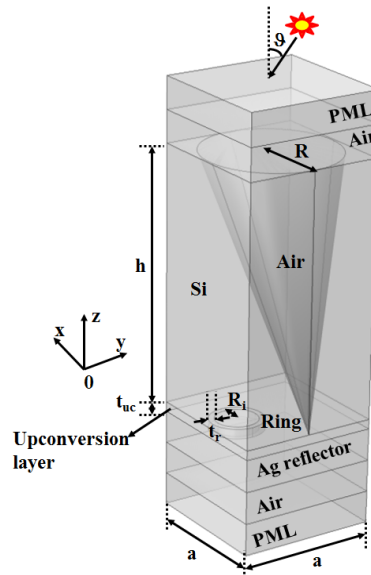

Fig. 1. A unit cell of the combined plasmonic and photonic crystal silicon solar cell structure based on a square lattice of slanted conical-pores in silicon and metallic core-shell rings. The up-conversion layer, in which the up-converter is doped, is sandwiched between the slanted cone PC and the Ag back reflector. The plasmonic core-shell ring resonator is integrated inside the up-conversion layer.

3. MAPD enhancement by a thin up-conversion layer

Remarkably, we find that even without any up-conversion, the presence of an up-conversion layer as a buffer region between the silicon active region and the metallic back reflector increases the MAPD relative to the same structure without the buffer. While a metallic back

reflector provides reflection of initially unabsorbed sunlight back into the light-trapping region, it is also a course of parasitic optical absorption loss. This parasitic loss is more pronounced when the back reflector is textured to provide additional light trapping. Using a buffer layer between the active layer and the back reflector can reduce the parasitic loss [52,53]. There is a tradeoff between plasmonic resonance enhanced photo-current generation and optical absorption loss due to Joule heating of the metal [54]. By optimizing MAPD with respect to UC thickness, we find the optimal UC thickness $t_{uc} = 60$ nm as seen in Fig. 2. The resulting MAPD of 36.41 mA/cm^2 corresponds to an integrated absorption efficiency of 89.14%. This exceeds both the Lambertian limit (33.26 mA/cm^2) and the slanted conical-pore PC without the buffer (35.47 mA/cm^2). Figure 3(a) depicts the absorption spectra of (i) the cell with the UC layer (red line), (ii) the Lambertian limit (green line) and (iii) the bare cell without the UC layer (black line). Figure 3(b) confirms that the buffer UC layer reduces absorption loss in the back reflector. The black line (corresponding to the absorption loss in the back reflector of the bare cell without the UC layer) is well above the red line (corresponding to loss in the cell with the UC layer).
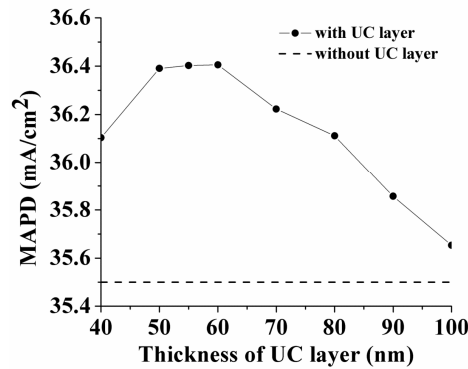

Fig. 2. The MAPD of the cell (from above-bandgap solar absorption) with and without the up-conversion (UC) buffer layer as a function of the buffer layer thickness.
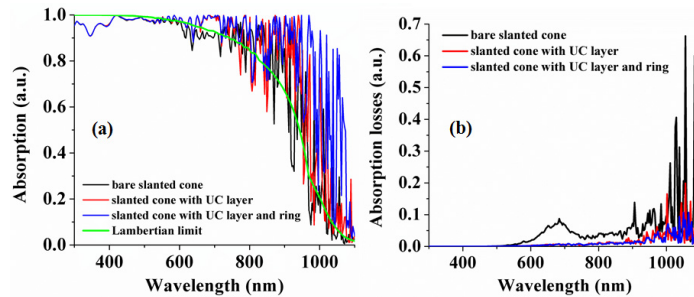

Fig. 3. (a) The absorption spectra of (i) the bare slanted conical pore photonic crystal-based solar cell without the UC layer (black line) and (ii) the cell with the UC layer (red line), (iii) with both the UC layer and the core-shell ring (blue line), and (iv) the Lambertian statistical ray trapping limit (green line). (b) The absorption loss as a function of wavelength in the back reflector of (i) the bare cell without the UC layer (black line), (ii) the cell with the UC layer only (red line) and (iii) the cell having both the UC layer and the core-shell ring (blue line).

4. Enhanced light trapping and plasmonic field enhancement by core-shell rings

In conventional single-junction solar cells, failure to absorb photons below the bandgap of the active materials, (i.e. GaAs or Si) limits the power conversion efficiency below the Shockley-Queisser limit of about 32% [38]. Up-conversion of these low-energy photons provides an avenue to surpass this thermodynamic efficiency limit. However, up to now UC materials

have had very limited impact in photovoltaic devices due to their extremely weak and narrowband near-IR absorption. Therefore, it is crucial to design solar cell architectures that deliver very high light intensities in the IR to the UC material and to broaden the spectrum of up-conversion.

Architectures to locally enhance the electromagnetic field and other lanthanide ions serving as sensitizers to the Erbium up-convertor have attracted much attention [55–58]. Plasmonic materials have been employed in poorly absorbing solar cells to enhance the absorption of above-bandgap photons. Engineering the metallic back reflector of solar cells with triangular gratings to couple into surface plasmon modes has revealed broadband absorption enhancement in the wavelength range of 600-800 nm [50]. Localized surface plasmon resonances excited in plasmonic gratings or nanoparticles embedded in the active material have provided absorption and near-field enhancement in the wavelength range above 600 nm in thin-film organic solar cells (OSCs) [9,51]. An integrated absorption efficiency of an ultra-thin (33 nm) OSC was increased from 30% up to 47% with embedded nanoparticles in the active layer [51]. In addition to enhancing the absorption of above-bandgap photons, plasmonic resonances can provide strong light concentration essential for nonlinear optical up-conversion [30,44,59].

Recently, a new method for broadband UC luminescence of Er-nanocrystals using organic IR dyes as sensitizers has been reported [42]. Here, dye molecules act as antennae to absorb incident light over a broad band (say 1100 nm-1500 nm) and then transfer their excitation energy to up-converting nanoparticles. Then, the up-converted photon energy is transferred radiatively or non-radiatively to the active layer of solar cells. However, a light focusing architecture is crucial to ensure a significant yield from this chain of relatively weak processes. In the present paper, we suggest a route to improve the UC efficiency of the up-converter (β-NaEr$_{0.2}$Y$_{0.8}$F$_4$) in the spectral range 1400-1600 nm through plasmonic enhancement of near-field light intensity in the up-converter. This is achieved using core-shell rings with up-conversion material in the core of a silver shell. Previously, dielectric-metal core-shell rings have been used for plasmonic waveguides in the optical communication band [60], providing broadband electric field enhancement in the spectral range of 1000-2000 nm. These localized surface plasmon resonances (LSPR) can be spectrally tuned by varying the structural dimension of the rings. Accordingly, we tune the plasmonic resonances to coincide spectrally with the wavelength of highest UC quantum yield of the up-converter.

Starting with the optimized slanted conical-pore PC and UC layer below, we find the optimal ring structure and position to get the highest MAPD and integrated absorption efficiency. This optimization is performed considering only the absorption of above-bandgap sunlight. We keep the height of the ring equal to the UC layer thickness t_{uc} = 60 nm. Using an inner radius R_i = 120 nm and a ring thickness t_r = 35 nm, we find a MAPD of 37.92 mA/cm^2 (corresponding to the integrated absorption of 90.62%) as shown in Fig. 4. This optimized MAPD is realized when the ring center is located at (x,y) = (a/2,a/4) inside the UC layer. The corresponding absorption spectrum plotted in Fig. 3(a) (blue line) surpasses the Lambertian limit and that of the slanted conical pore PC with and without the UC layer. It is seen that at wavelengths near 750 nm nearly perfect above-bandgap photon absorption is achieved. This photonic crystal light-trapping mostly occurs in bright hot spots in the electric field profiles, as shown in Figs. 5(a) and 5(b). This increased local electromagnetic density of states provides enhancement in the rate of up-converted emission (from two-photon absorption at wavelengths near 1500 nm) and improves the overall photo-current generation efficiency. The greatest absorption enhancement is found in the spectral range of 900-1100 nm where combined plasmonic and photonic crystal resonances occur. The normalized electric field intensity corresponding to the resonant peak in the absorption spectrum at λ = 1032 nm is shown in Figs. 5(c) and 5(d). Here, bright hot spots (corresponding to the high light intensity) are observed in the silicon light-trapping region and at the silicon/ring interface. This light-trapping enhancement persists (see Fig. 6) even as the cone height is reduced to 800 nm

(equivalent bulk silicon thickness of 500 nm). However, this enhancement is lost if two rings are placed symmetrically on either side of each conical pore due to higher parasitic optical absorption loss in the rings and the Ag back reflector.
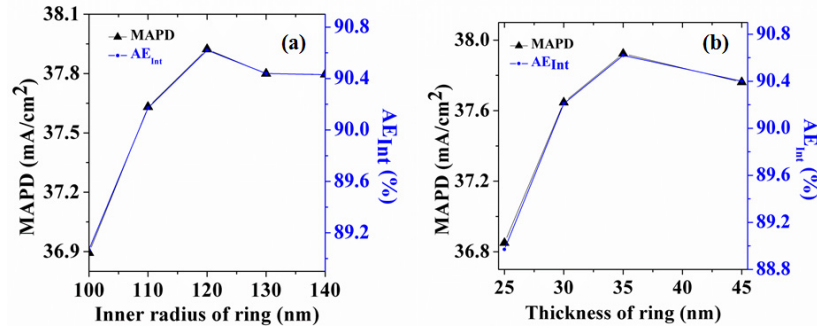

Fig. 4. Short circuit current optimization for the slanted conical pore PC cell with lattice constant a = 850 nm, cone radius R = 425 nm, and up-conversion layer thickness t_{uc} = 60 nm for various core-shell ring geomeries: (a) MAPD as a function of inner radius for fixed ring thickness t_r = 35 nm (b) MAPD as a function of ring thickness for fixed inner ring radius R_i = 120 nm. The maximum short circuit current is obtained for inner ring radius R_i = 120 nm and thickness t_r = 35 nm.
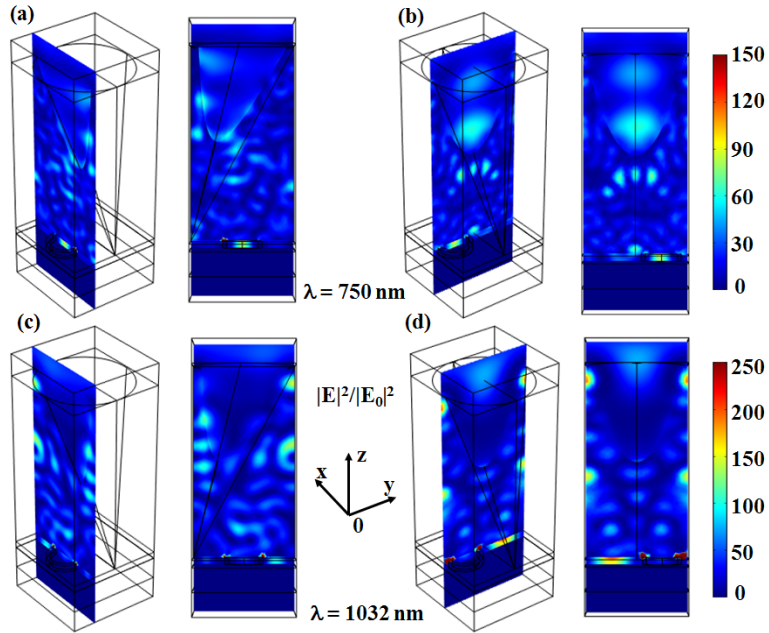

Fig. 5. Normalized electric field intensity at certain wavelengths in the chosen xz plane and yz plane view, respectively. The peak intensity enhancement in the photonic crystal at 750 nm and 1032 nm is about 100 and 200, respectively.
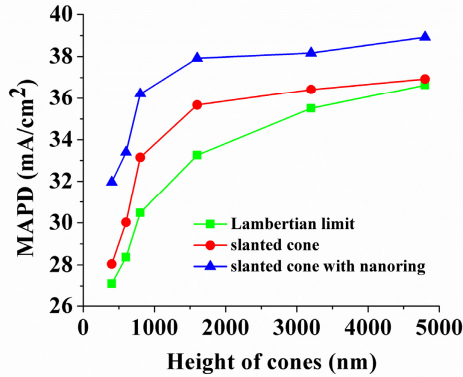
Fig. 6. The MAPD of slanted concial pore PC's as function of pore depth with and without plasmonic core-shell ring resonators. Here the ratio of pore height to equivalent bulk thickness of silicon is about 1.6. On the same graph, we plot the Lambertian limit for (nonporous) films of thickness equal to the pore height/F where F~1.6. In other words, the Lambertian films contain an equal amount of silicon to the photonic crystal films to which they are directly compared. At the pore height of 800 nm (500 nm of Si), the MAPD is reduced by only about 5% from the MAPD at the pore height of 1600 nm (1 micron of Si). This suggests the possibility of high-efficiency, thin-film silicon solar cells with equivalent bulk thickness of 500 nm.

An important aspect of solar cell performance is the ability to absorb most available sunlight at off-normal incidence for both transverse electric (TE) and transverse magnetic (TM) polarizations over a broad angular range. For TE modes, the electric field vector is perpendicular to the plane of incidence whereas for TM modes, the electric field vector is parallel to the plane of incidence. Figure 7 depicts the MAPD of the cell with and without the core-shell ring under both TE- and TM-polarized illuminations. It is seen that no substantial degradation in the MAPD of the bare slanted conical pore PC cell without the ring happens at least up to 60° for both polarizations. The TM-polarized light yields stronger MAPD than that of TE over a wide angular range. Remarkably, in the TM channel, certain oblique incidences yield better solar absorption than normal incidence. Clearly, in the presence of the plasmonic ring resonator, the MAPD is enhanced relative to that of the silicon photonic crystal alone for all angles and both polarizations. A major advantage of including the core-shell ring is the enhancement of the field intensity of sub-bandgap sunlight in the up-converter in regions near the ring.
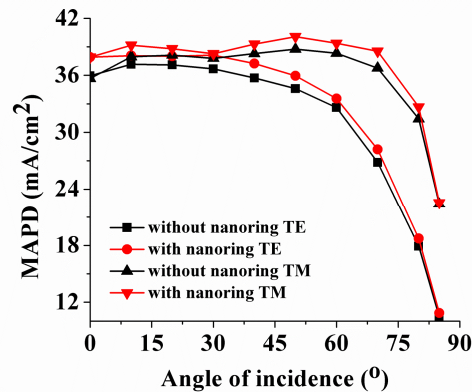

Fig. 7. Angular response in term of the MAPD of the slanted conical pore PC cell with and without plasmonic core-shell ring resonators for TE- and TM-polarized light illuminations.

In Fig. 8, we demonstrate the sub-bandgap absorption enhancement of the up-converter when the ring is placed inside the UC layer. The absorption here is averaged over the volume of the UC layer and the enhancement is compared to the bare cell without the ring. We find at certain resonances that the averaged absorption is enhanced by a factor of 50 relative to the UC cell without the ring. Moreover, the intensity enhancement at the wavelength of 1500 nm relative to the incident sunlight (The incident plane wave is assumed to be E = 1 V/m) is up to factor of 1400 times more (see Fig. 9). The same figure shows the intensity enhancement relative to the incident sunlight at two chosen resonant wavelengths. The bright hot spots of intensity enhancement are the regions of best up-conversion. Here the light intensity reaches that of about 1400 suns in the absence of an external solar concentrator. High-yield up-conversion is expected if in fact an external solar concentrator, providing about 100 suns, is placed above our combined plasmonic and photonic crystal solar cell.
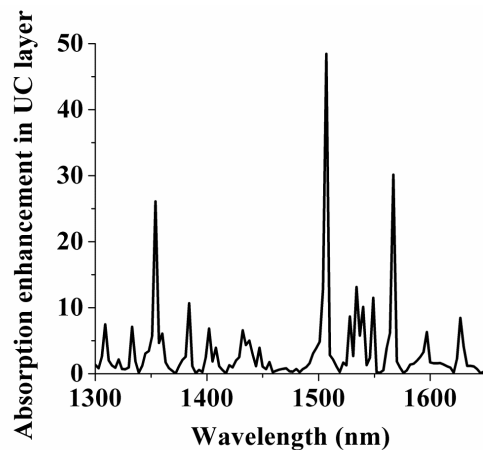

Fig. 8. Ratio of the sub-bandgap solar absorption (integrated over the up-conversion volume) in the 60 nm thick up-conversion layer with and without the plasmonic core-shell ring resonator.
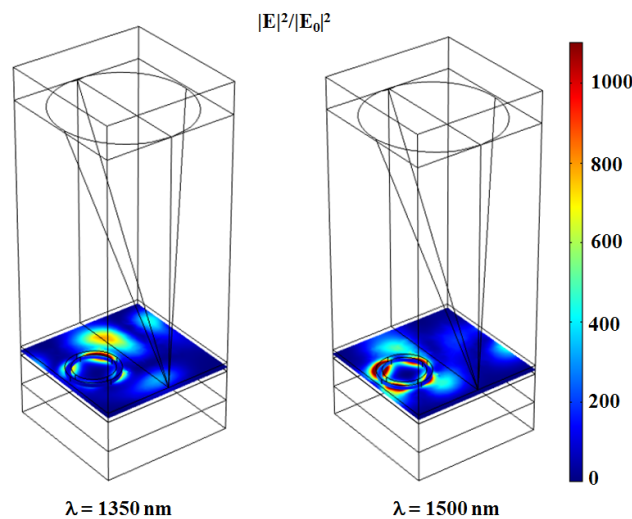

Fig. 9. Normalized electric field intensity in the up-conversion layer caused by the core-shell ring at resonant wavelengths of 1350 nm and 1500 nm. The peak intensity ratio for 1500 nm is about 1400. Here $|E_0|^2$ is the incident solar intensity at the chosen wavelength.

5. Conclusions

In this paper, we have demonstrated the synergetic interplay between photonic crystal and plasmonic resonances to (i) enhance solar light trapping and absorption of above-bandgap photons in thin-film crystalline silicon, (ii) enhance sub-bandgap light absorption in an ultra-thin-film of up-conversion material sandwiched between the silicon active region and a back-reflector, and (iii) deliver very high sunlight intensities at relevant wavelengths to drive a chain of broadband up-conversion events. Our up-conversion layer also acts as a buffer layer to reduce parasitic optical absorption loss in the back reflector, resulting in above-bandgap absorption enhancement of up to 4.7% relative to the same solar cell without the buffer layer. Our numerical simulations focused on an equivalent bulk thickness of 1000 nm of silicon in which a MAPD of roughly 38 mA/cm^2 was demonstrated, corresponding integrated absorption efficiency of about 91%. However, the most cost-effective volume of silicon was found at an equivalent bulk thickness of 380 nm (600 nm conical pore depth) for which the MAPD is reduced by less than 12% from the above value. In all cases, the light-trapping capacity of our combined plasmonic and slanted conical-pore PC considerably exceeds the Lambertian statistical ray trapping limit over the wavelength range from 300 nm to 1100 nm. Our plasmonic core-shell ring resonator inside the up-conversion layer of the slanted conical-pore PC provided a MAPD enhancement of 6.7%. More importantly, it provides sunlight intensity enhancements over the 1000 nm −1500 nm range for absorption by IR dyes and more than a factor of 1000 intensity enhancement at the wavelength for two-photon absorption and up-conversion by Erbium. When combined with an external solar concentrator providing 100 suns, significant up-conversion of sub-bandgap sunlight is possible. We also investigated the variation of the MAPD, influenced by the core-shell ring, with respect to the angle of sunlight incidence under both TE and TM polarizations. Excellent solar light trapping in addition to large absorption enhancement was found over a wide angular range of 0 ° - 60° for both polarizations. These results suggest that the careful positioning, both spatially and spectrally, of plasmonic and photonic crystal resonances may provide a route to thin-film silicon solar cells with power conversion efficiencies approaching 30%.